PHYSICAL REVIEW B VOLUME 13, NUMBER 2 15 JANUARY 1976

Use of hydrogenation in structural and electronic studies of gap states in amorphous germanium*

G. A. N. Connell and J. R. Pawlik

Gordon McKay Laboratory, Division of Engineering and Applied Physics, Harvard University, Cambridge, Massachusetts 02138

(Received 17 July 1975)

A method of hydrogenating sputtered amorphous Ge has been developed for systematically studying the variation of the electronic properties with the number of dangling bonds. The role of incorporated hydrogen was established by the correlation of x-ray diffraction, electron paramagnetic resonance, and optical spectroscopy. A model for the logistics of incorporation of hydrogen was also developed and compared with experiment. The origin of the states in the gap of partially coordinated amorphous Ge was traced to the dangling bonds on void surfaces. These states span a large fraction of the energy gap of partially coordinated material, to the extent that transitions between them completely determine the optical absorption below photon energies of about 0.6 eV. (Optical absorption, across the band gap itself, in fully coordinated material, does not occur until about 1 eV.) However, the electron spin density is much smaller than the dangling-bond density, indicating that electrons most often pair to form weak molecular bonds or bipolarons on the void surfaces. Finally, the temperature dependence of the EPR linewidth appears to be correlated with the temperature dependence of the nonactivated conductivity.

I. INTRODUCTION

In recent years, the relationship between the gross features of the electronic and vibrational densities of states in tetrahedrally bonded amorphous semiconductors and the topological and quantitative disorder has been rapidly established.[1] On the other hand, progress towards an understanding of the nature of the electronic states near the valence and conduction band edges has been slow. Mott's original description of the localization of electrons in the tails of the valence and conduction bands of a disordered but completely coordinated network, as a result of rapid potential fluctuations,[2] has been questioned at several levels. Cohen and coworkers[3] have argued that the transition between localized and itinerant states is not marked by an abrupt change in electron mobility at an energy given by the Anderson criterion.[4] Rather, the mobility starts to rise slowly at this energy. Nevertheless, the distinction between a mobility gap and a band gap and the qualitative predictions of the Mott model remain. Phillips,[5] Van Vechten,[6] Emin,[7] and Anderson,[8] in contrast, each argue that localized electrons couple to the network and can lower their energy by inducing local network deformations. Thus a tail of localized states in a rigid network is unstable against atomic displacements and the tails of localized states in the gap of the equivalent deformable network may be modified or even removed, depending on the strength of the electron-phonon coupling for the localized states involved. In addition, Anderson envisages that the deformations may occur in a way that allows electron pairs to form[9] and then any possibility of Curie or Pauli paramagnetism occurring is also removed.

Clearly, experimental input is required to elucidate the appropriate approach to the problem in the tetrahedrally coordinated materials, but unambiguous data have been difficult to obtain. For example, the presence of defects within the network gives rise to gap states[10] and confuses the investigation of the existence and extent of any band tails, the existence and sharpness of any mobility edge between localized and extended states, and the numeric value of the energy gap itself in fully coordinated material. Yet, the preparation of fully coordinated material has either not been possible or has not been demonstrated with certainty by structural measurements,[11] although in some cases perhaps it has been indirectly suggested by other measurements. For example, in earlier work on sputtered amorphous Ge, it was shown that a substrate temperature of 325 °C during deposition, produces a comparatively high density of $5.18 \pm 0.03\,\mathrm{g/cm^3}$ and a coordination number of 3.92 ± 0.1,[10] but, even so, a dangling-bond density of approximately 2.5 at.% is still possible. Thus to date experimental data on the electronic states in and near the gap region cannot necessarily be assigned to the intrinsic electronic states of fully bonded amorphous Ge.

In this work, the radical approach of Lewis *et al.* has been followed.[12] Hydrogen, with its single electron and its small covalent radius, can be used to compensate individual dangling bonds on the void surfaces of amorphous Ge, and the variations of the electronic properties with hydrogen coverage can be determined. Thus, the density of electronic states of fully bonded but hydrogenated amorphous Ge, which near the gap will resemble that of fully coordinated material, can in principle be established. The advantages of this new technique over the traditional approaches to minimize the number or effects of dangling bonds, i.e., annealing or using an elevated substrate temperature during deposition, are numerous. The traditional methods in addition to modifying the void structure also modify the network itself and both effects contribute inseparably to the changes of the properties.[10,13] Furthermore, it is difficult to measure directly whether all dangling bonds have been removed after a certain thermal treatment. In contrast, hydrogenation does not suffer from these deficiencies. Hydrogen may be added till saturation of the void surfaces occurs and the properties can be observed at this juncture. Moreover, a study of the effects of annealing on the properties of saturated material demonstrates the effects of network reorganization.

The results of this investigation are presented in two papers: this paper contains the structural, optical, and magnetic properties and the other authored by Lewis contains the transport properties.[14] The aim of this paper is twofold. First, by correlation of x-ray diffraction, electron paramagnetic resonance, and infrared reflection and transmission data the role of hydrogen incorporation in the films is established. Second, from optical-absorption data at photon energies in the region of the band gap and the foregoing results the origin of the electronic states in both defective and fully coordinated amorphous Ge is determined. The experimental methods are described in Sec. II, the results presented in Sec. III are interpreted in Sec. IV and the paper is summarized in Sec. V.

II. EXPERIMENTAL METHODS

A. Material preparation

The basic preparation technique was first described by Lewis *et al.*[12] Here that summary is amplified. Amorphous Ge, $Ge_{1-x}H_x$, $Ge_{1-x}D_x$, and $Ge_{1-x}H_{0.5x}D_{0.5x}$ films and Si and $Si_{1-x}H_x$ films, approximately 25-μm thick, were made by rf sputtering in a Vacuum Industries 2305 Diode Sputtering System. Base pressures of 5×10^{-7} Torr, shown to be water vapor by residual gas analysis, were obtained by dry turbomolecular pumping, before introducing 5×10^{-3} Torr of 99.9995% pure Ar. Hydrogen or deuterium incorporation into the sputtered material was achieved by adding a partial pressure p_h of between 5×10^{-5} and 8×10^{-4} Torr of 99.999% pure H_2 or D_2 to the Ar. Both Ar and H_2 or D_2 pressures were stable to within ±10% during the period of the run, typically 24 h. Films grown at $p_h \gg 10\times10^{-4}$ Torr were rough and mechanically unstable. However, they had approximately the same room-temperature conductivity as films grown at $p_h = 8\times10^{-4}$ Torr,[12] and thus they were not used for this work. The substrates, ultrasonically precleaned and degreased, and the target were separately cleaned *in situ* before each run began by reverse sputtering at 0.5 W/cm^2 for 5 min and forward sputtering at 2 W/cm^2 for 5 min, respectively. Using optical grade polycrystalline Ge and Si targets 5 in. in diameter sputtering rates of about 3 Å/sec were achieved with 2 W/cm^2 of forward power and a source-to-substrate distance of 10 cm. High resistivity float glass slides (Corning 7059), polished Be foils, 0.005-in. thick, and cleaved KBr slabs were used throughout the work as substrates. When unsupported samples for EPR or density measurements, for example, were required the Be could be dissolved in a 10 Vol % HCl solution. Amorphous films were prepared at two substrate platform temperatures T_s nominally 25 ° and 250 °C,[15] and were measured in both their as-prepared state and after an anneal of 60 min at $T_a = 250$ °C in a vacuum of 1×10^{-5} Torr.

An attempt was made to incorporate hydrogen into unhydrogenated material by exposing a film *in situ* to a $p_h = 1.3\times10^{-2}$ Torr hydrogen plasma, maintained by an rf power of 30 W. However, even after an exposure of 1.5 h, less than 1 at.% of hydrogen resided in the film. Films subjected to similar exposures during growth contained approximately 10 at.% of hydrogen.

B. Structural measurements

Two direct measurements of the dependence of structure on hydrogen incorporation were made. In the first, the mass density ρ_0 was determined by weighing an unsupported sample in air and toluene. In the second, the coherently scattered x-ray intensity, $I(s)\,[1 \leq s \leq 15$ Å^{-1}, $s = (4\pi/\lambda)\sin\theta]$, was observed in reflection from films on Be substrates by Lewis *et al.*[12] The details of the experimental techniques[16] and a preliminary report of the results have been given elsewhere.[12] The interpretation of the results is presented here.

An indirect structural measurement was also made. An earlier study indicated that the concentration of argon in sputtered amorphous Ge films was proportional to the total void volume provided that deposition rates and biasing conditions were fixed.[16] The argon concentration thus represents a convenient measure of the total void volume in material prepared at different hydrogen partial pressures. In this work the films were analyzed by electron microprobe analysis using techniques for absolute measurements that were described previously.[10] The error in the measured concentrations is ±10%.

C. Optical measurements

Optical absorption data were obtained with photon energies ranging from 0.03 to 1.5 eV. Below 0.5 eV a Perkin-Elmer Model 567 Double Beam Spectrometer was used with two specular reflectance accessories to obtain reflectance (R) and transmittance (T) data from samples deposited on KBr substrates. Below 0.15 eV, the absorption coefficient α was determined by the RT method.[17] With a sample thickness of $t \approx 25$ μm, the error in α is about 30 cm^{-1}. It should be emphasized that this technique by itself does not give reliable values of the refractive index n under the conditions used here, but from the photon energies of the maxima and minima in the transmitted or reflected intensity, and the sample thickness, determined by edge-on viewing at 1000× magnification, n can be determined separately to about 0.05. This value is held fixed in the calculation of α.

Absorption coefficients in the region of the absorption edge, which typically occurs above 0.5 eV, were determined from films on glass substrates in a versatile single-beam instrument described elsewhere[18] that is used for reflection, transmission, and ellipsometric measurements. Above $\alpha \approx 100$ cm^{-1}, or below, after numerical averaging of the interference fringes, the transmittance of films of thickness t is given by

$$T = \frac{(1-R_1)(1-R_2)(1-R_3)\,e^{-\alpha t}}{1-R_2R_3-e^{2\alpha t}(R_1R_2+R_1R_3-2R_1R_2R_3)}\ ,$$

where R_1, R_2, and R_3 are the reflectances of the air-film, film-substrate, and substrate-air interfaces, respectively.[19] For $\alpha \lesssim 5\times10^4$ cm^{-1}, the extinction coefficient k near 1 eV is very much less than n, so that R_1, R_2, and R_3 may be calculated directly from n and the substrate refractive index n_s. In the present case, the refractive index n was determined by ellipsometry or from interference fringes. A full description of the experimental techniques and precautions needed when making these measurements have been described previously.[18] Compounding the estimated errors in R_1, R_2, T, and t leads to an error in α of about 50 cm^{-1}.

This technique was also used with films on KBr substrates for absorptions that occurred at energies below 0.5 eV yet above 0.15 eV. However, when $\alpha > 100$ cm^{-1}, the refractive index in the region of the absorption was estimated from its values at lower and higher energies.

D. Electron paramagnetic resonance measurements

Spin susceptibility and linewidth measurements between 100 and 350 K were performed with a Varian E-9 spectrometer, equipped with an E-231 multipurpose cavity and a temperature-recalibrated Varian E-257 variable temperature accessory. Additional linewidth measurements were obtained at 4.2 and 77.4 K, using a Varian E-245 liquid-helium accessory and a Varian E-246 liquid-nitrogen Dewar, respectively. Preliminary measurements were made on samples deposited on spin-free quartz rods,[12] but better sensitivity and accuracy was obtained in this report from unsupported flakes encapsulated in a helium atmosphere within Wilmad 707-*SQ* quartz sample tubes. Calibration spectra were obtained from a 0.1% pitch in KCl standard, supplied by Varian and having $(3\pm0.75)\times10^{15}$ spins/cm. The material was held in a quartz tube, similar to those used for the samples, and thus the large calibration error that can arise from different deformations of the microwave field pattern by the different quartz inserts in the calibration and sample experiments was minimized. The earlier measurements of the susceptibility of material on quartz rods[12] were systematically high for this reason.

At the typical microwave powers P of 10–15 mW, the samples were nonsaturating and the detector diode was in its linear region of operation. The amplitude of the modulation field, $H_m(x) = H_m(0) \times \cos(\pi x/2a)$, where x is measured from the center of the cavity along the axis on which the sample is inserted, and $2a$ is the length of the cavity, was less than 9% of the sample linewidth at all x. Thus the output voltage of the spectrometer, which is detecting the voltage reflected from the cavity that is in phase with H_m, is given by

$$y'(\omega, H) = KGP^{1/2}\,QH_m(0)\,\eta V_s\left(\frac{\partial\chi''(\omega, H)}{\partial H}\right)_\omega\ ,$$

where K is a system constant, G is the detector gain, Q is the cavity quality factor when the sample is not at resonance, ω is the microwave frequency, V_s is the volume of the sample, and H is the static magnetic field. For a line sample typical of those used here η, which is related to the filling factor, is given by

$$\eta = \frac{1}{V_s}\int_{V_s}\left(\frac{H_1(x)}{H_1(0)}\right)^2 \frac{H_m(x)}{H_m(0)}\,dV\ ,$$

where $H_1(x) = H_1(0)\cos(\pi x/2a)$ is the amplitude of the microwave field along the sample axis for the TE$_{102}$ mode of the E-231 cavity. Finally the imaginary part of the complex microwave magnetic susceptibility per unit volume χ'' is related to the static magnetic susceptibility per unit volume χ_0, in unsaturated lines as follows:

$$\chi''(\omega, H) = \pi\chi_0 g\mu_B H \mathcal{L}(\omega - g\mu_B H/\hbar)/2\hbar\ ,$$

where $\mathcal{L}(\xi)$ is the line-shape function normalized to unit area with respect to ξ and μ_B is the Bohr magneton. Thus

$$A \equiv \int_0^\infty\int_0^H y'(\omega, H')\,dH'\,dH = \tfrac{1}{2}\pi KGP^{1/2}\,QH_m(0)\eta V_s H_0\chi_0$$

is obtained, where H_0 is the value of H at maximum absorption.

The procedure for the determination of $\chi_0(T)$ is now straightforward. Q is monitored as a function of temperature for all samples by a method owing to Singer[20]; a small synthetic ruby (Al$_2$O$_3$ with

0.5 wt% Cr^{3+}) was attached to a cavity wall during the measurement of the temperature dependence of ΔH_{pp}, the magnetic field separation between the extrema in y', and $y'_m \equiv \frac{1}{2}(y'_{\max} - y'_{\min})$. Thus the ruby remains at ambient temperature during the experiment and y'_{mr}, the y'_m of its resonance at $g \approx 2.3$, is proportional to Q. It is then easily shown that A_Q, the value of A normalized to constant Q, is

$$A_Q = l \frac{y'_m}{y'_{mr}} \Delta H^2_{pp} = \int_0^\infty \int_0^H \frac{y'(\omega, H')}{y'_{mr}} dH' \, dH \quad ,$$

where l is a constant for a particular line shape. For example, it is 3.628 for a Lorentzian line and 1.033 for a Gaussian line. It should be noted that the g values of ruby and amorphous Ge are sufficiently different that overlap of their lines can be neglected at fields within a few ΔH_{pp} of resonance. This is not true in the tails of the Ge resonance and thus l cannot be determined in a Singer experiment. However, although Q cannot be monitored simultaneously, l can be found from the numerical integration of $y'(\omega, H')$ and the corresponding values of y'_m and ΔH_{pp} when the ruby is absent from the cavity. The integrations were limited for experimental reasons to a magnetic field interval of $12 \Delta H_{1/2}$, where $\Delta H_{1/2}$ is the full width at half-maximum in the magnetic field of the absorption, and χ_0 may be somewhat underestimated as a result. For example, these limits of integration would include 94.7% of the area of a Lorentzian and close to 100% of the area of a Gaussian. Nevertheless, the combination of these two experiments permits a reasonable estimate of A_Q.

A_Q may now be determined for the sample $A^s_Q(T)$ and for the calibration material $A^c_Q(300)$. The sample susceptibility $\chi^s_0(T)$ is then given by

$$\chi^s_0(T) = \frac{A^s_Q(T)}{A^c_Q(300)} \left(\frac{P_c}{P_s} \right)^{1/2} \frac{G_c}{G_s} \frac{H^c_m(0)}{H^s_m(0)} \frac{H^c_0}{H^s_0} \frac{\eta_c}{\eta_s} \frac{V_c}{V_s} \chi^c_0(300) \; ,$$

where the subscripts s and c designate the sample and calibration standard, respectively. In practice, it was found that l was only weakly temperature dependent (although a failure to recognize this dependence could lead to an erroneous temperature dependence of χ_0) and it was sufficient to interpolate between l values at a few selected temperatures to determine $A_Q(T)$ at many temperatures. These procedures were observed to reproduce the susceptibility of a given material to typically ± 6%, when measurements were made with masses varying by a factor of about 7. Finally, it was noted that $y'(\omega, H)$ often had a small symmetric component resembling dispersion in samples for which $y'(\omega, H)$ was known to be antisymmetric. This can be caused by slight off-axis positioning of the sample, by insufficient automatic frequency control (AFC) gain, or by a small misalignment of the microwave bridge, for example. Accordingly, the $y'(\omega, H)$ data, presented later, was antisymmetrized to remove any dispersive component. This has no effect on the experimental value of χ_0, but is believed to give the best estimate of $\mathcal{L}(\omega - g\mu_B H/\hbar)$.

III. RESULTS

A. Localized phonon modes and oxygen and hydrogen content

The effect of oxygen on the optical spectrum of amorphous Ge below 0.15 eV has been described previously.[18] It was found that with oxygenation an absorption peak develops at 0.09 eV. A similar experiment on amorphous Si has now demonstrated that the corresponding vibrational mode occurs at 0.115 eV. These features have therefore been used as a measure of the oxygen content of the films investigated. Figure 1 shows the transmission through two Si films for wave numbers between 700 and 1200 cm^{-1}. The attenuation of the interference fringes near 900 cm^{-1} in the thinner film ($t \approx 13$ μm) is the result of leaking air into the sputtering system at a partial pressure of 2×10^{-6} Torr during deposition. In the thicker film ($t \approx 15$ μm), made under normal conditions, the attenuation observed is comparable to the accuracy of the measurement. Nevertheless, an analysis of the data indicated a maximum absorption coefficient owing to Si-O vibrations of 50 ± 30 cm^{-1}. Using the data of Kaiser *et al.* for the absorption from Si-O pairs in crystalline Si,[21] an oxygen concentration of 250

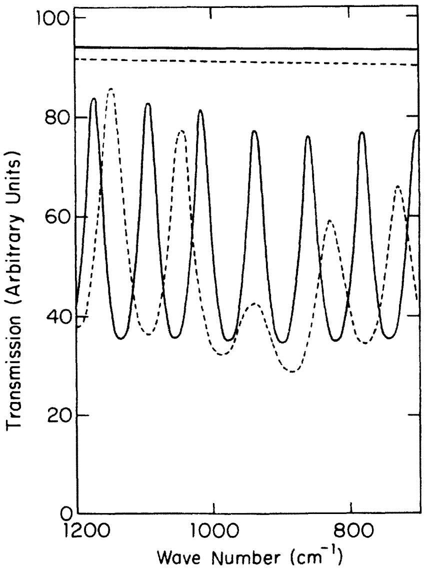

FIG. 1. Optical transmission of Si films sputtered in pure argon (straight line) and with an air partial pressure of 2×10^{-6} Torr (dashed line). Oxygen produces an absorption near 900 cm^{-1} in the second film. Lines corresponding to 100% transmission are also indicated.

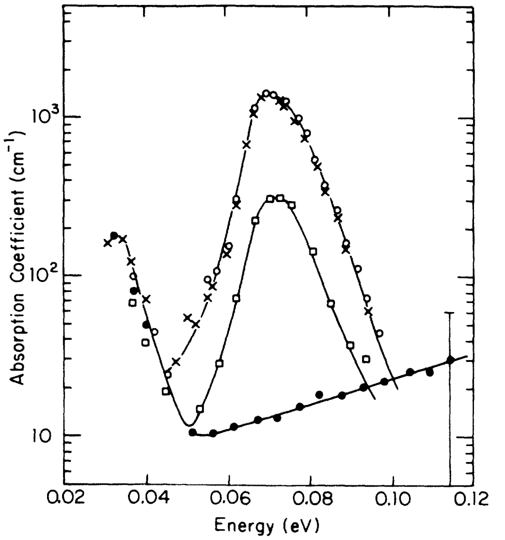

FIG. 2. Absorption coefficient vs photon energy for $Ge_{1-x}H_x$ films: $x=0$ (●●●), $x=0.01$ (□□□), and two films with $x=0.05$ (××× and ○○○). Note the asymmetry of the absorption at large hydrogenation.

±150 ppm was determined. A mass-spectrographic analysis of the Si target material indicated 350 ppm. The situation for amorphous Ge was similar, but in this case no absorption at 0.09 eV attributable to Ge-O bonds could be detected in unhydrogenated material, as shown in Fig. 2. It was therefore concluded making use of data of Kaiser *et al.* on Ge-O pairs in crystalline material[22] that the oxygen concentration on the amorphous Ge films was significantly less than 300 ppm. Similar experiments on hydrogenated material gave the same result.

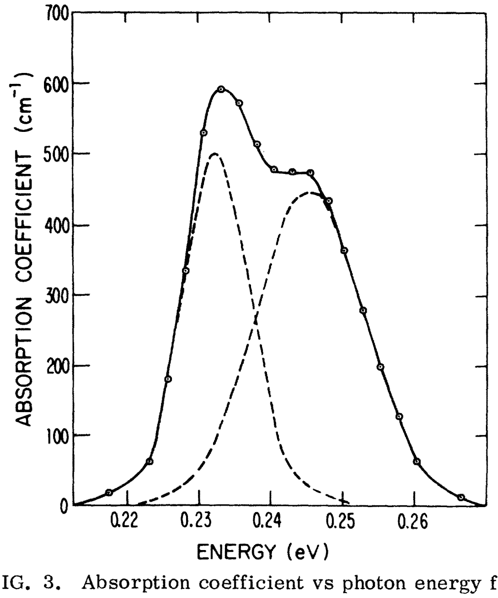

FIG. 3. Absorption coefficient vs photon energy for a $Ge_{1-x}H_x$ film $F(8.0)$. Absorption doublet is deconvoluted into two components centered at 0.23 and 0.245 eV.

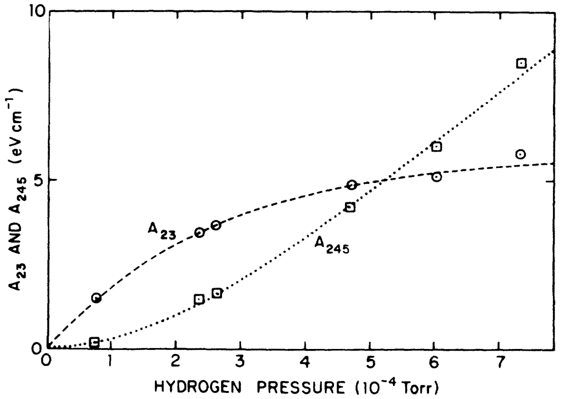

FIG. 4. Integrated intensity of absorption peaks at 0.23 eV (A_{23}) and 0.245 eV (A_{245}) vs hydrogen partial pressure during sputtering for $Ge_{1-x}H_x$ films. Theory of Sec. IV B is represented by the broken lines.

The effect of hydrogen incorporation on the optical spectrum below 0.5 eV was twofold: absorption peaks developed near 0.07 and 0.23 eV but the background absorption and the long-wavelength refractive index decreased. In this section the appearance of the absorption peaks will be discussed. The reduction in background absorption and refractive index, which occur through changes in the electronic density of states, will be discussed in Sec. III D.

Typical absorption spectra of hydrogenated material are shown in Figs. 2 and 3. The highest energy peak of the Ge phonon spectrum is seen at 0.035 eV in all films. In contrast the total integrated intensity of the bands near 0.07 and 0.23 eV increased with the hydrogen partial pressure p_h that was used during the deposition process. Deuterated material had a similar series of absorption bands which occurred near 0.0515 and 0.165 eV. A comparison of these two sets of data with the spectra of gaseous GeH_4 and GeD_4,[23] liquid $GeBr_3H$,[24] and $GeCl_3D$,[25] indicates that the local Ge-H and Ge-D bond bending (0.07 and 0.0515 eV, respectively) and bond stretching (0.23 and 0.165 eV, respectively) modes were observed rather than new electronic transitions. We expect that the similar absorptions in amorphous Ge, made either by electrolysis[26] or by rf decomposition of germane,[27] have the same origin.

In Fig. 3, it is clearly seen that the 0.23-eV feature in hydrogenated material is a doublet as is the corresponding feature in deuterated samples. The dependence of its separate components on p_h is shown in Fig. 4. The integrated intensity of the 0.23-eV peak A_{23} initially rises rapidly but appears to asymptote when $p_h \gtrsim 2\times10^{-4}$ Torr. On the other hand, the integrated intensity of the 0.245-eV band

A_{245} at first rises slowly but grows rapidly throughout the remaining range of p_h studied. Although the clear experimental resolution of the 0.07-eV band into two peaks was never achieved, the distinct asymmetry of the line at high p_h (see Fig. 2) is strongly suggestive of a similar interpretation. A deconvolution of the data shown in Fig. 2 for $p_h = 5\times10^{-4}$ Torr leads to separate lines at 0.07 and 0.0775 eV, which, moreover, have roughly the same relative weight as $A_{23}:A_{245}$ in a similar film. We conclude therefore that hydrogen incorporation results in two final-state configurations that have different excitation energies for bending and stretching modes.

The vibrational modes in $Si_{1-x}H_x$ occurred at 0.079, 0.247, and 0.258 eV and their intensities had exactly the same dependence on p_h as those of the corresponding modes in $Ge_{1-x}H_x$. Evidently the mechanism of hydrogen incorporation is identical in both amorphous materials. Furthermore, the vibrational modes in $Ge_{1-x}H_{0.05x}D_{0.05x}$ appeared to be a superposition of the modes in $Ge_{1-x}H_x$ and $Ge_{1-x}D_x$ but with an intensity reduced as expected by $\frac{1}{2}$. The absence of an additional third absorption in the region of the bond-bending mode is taken to indicate that the higher-energy component in $Ge_{1-x}H_x$, for example, that grows rapidly in intensity at large p_h is not induced by interactions between hydrogen atoms in the material. This point will be taken up again later.

When hydrogenated material ($T_s = 25$ °C) was subjected to an anneal at 250 °C for 60 min, no clear changes in the positions or oscillator strengths of the Ge-H modes were observed. However, by measuring directly the difference between the transmissions of unannealed and annealed samples a small transfer of oscillator strength from A_{23} to A_{245} could be detected in the most hydrogenated material, although the total integrated absorption $A_{23}+A_{245}$ was maintained. $-\Delta A_{23} \simeq \Delta A_{245} \simeq 0.1 A_{23} \simeq 0.1 A_{245}$ in material sputtered with $p_h \approx 5\times10^{-4}$ Torr. Thus, hydrogen is not desorbed and Ge-H bonds are not broken by the annealing process used. Rather, the results suggest a network reorganization not necessarily accompanied by the breakage of Ge bonds in the vicinity of the voids.

The Ge-H vibrational spectrum of material made at $T_s = 250$ °C is qualitatively similar to that of corresponding material prepared at $T_s = 25$ °C. One quantitative difference is a reduced integrated intensity for a given p_h in $T_s = 250$ °C films. For example, when $p_h = 2\times10^{-4}$ Torr, $A_{07} = 17.0 \pm 1.5$ eV cm^{-1} for $T_s = 250$ °C and $A_{07} = 21.0 \pm 1.5$ eV cm^{-1} for $T_s = 25$ °C. However, within an experimental error of about 15% the ratio $A_{23}:A_{245}$ is unchanged. These last data together with the variation of A_{23} and A_{245} with p_h set stringent criteria for a model of hydrogen incorporation.

An estimate of the absolute hydrogen concentration in Ge-H bonds, as well as an accurate determination of the relative concentration of hydrogen in the different films, can be obtained from the total oscillator strength of either of the vibrational modes. Consider as a model for the Ge-H bonds distributed in the Ge matrix a dilute assembly of harmonic oscillators that consist of two atoms with effective charges $\pm e^*$ and reduced mass μ. Then the complex transverse dielectric constant is[28]

$$\tilde{\epsilon}(\omega) = \epsilon_0[1 + \omega_p^2/(\omega_t^2 - \omega^2 - i\gamma\omega)] \quad , \tag{1}$$

where

$$\omega_p^2 = (4\pi N e^{*2}/\mu\epsilon_0)[\tfrac{1}{3}(\epsilon_0 + 2)]^2 \quad ,$$

$$\omega_t^2 = \omega_0^2 - \tfrac{4}{3}\pi(Ne^{*2}/\mu)\tfrac{1}{3}(\epsilon_0 + 2) \quad ,$$

$$\omega_0^2 = k_0/\mu \quad ,$$

k_0 is the restoring constant, γ is a phenomenological transverse damping constant, N is the number of oscillators per unit volume, and ϵ_0 is the transverse dielectric constant of the matrix material. In the materials studied here the difference between ω_t and ω_0 can be ignored to a close first approximation in Eq. (1). Manipulation of Eq. (1) then gives

$$N = \frac{9}{2\pi^2}\frac{\mu}{e^{*2}(\epsilon_0 + 2)^2}\int_{\text{Absorption band}} \omega \,\mathrm{Im}\,\epsilon(\omega)\, d\omega \quad . \tag{2}$$

This expression can also be applied to a dilute assembly of GeH_4 molecules by replacing ϵ_0 by unity. Then from the published data relating N to the oscillator strength of either the bond-stretching or bond-bending mode of gaseous GeH_4,[23] the proportionality constant in Eq. (2) can be determined for each of the modes. The calculation is not quite straightforward, however. The point group of the GeH_4 molecule is T_d, so that the infrared-active stretching and bending modes are both triply degenerate (F_2 representations). On the other hand, the point group of a Ge atom tetrahedrally bonded to a hydrogen atom and three other Ge atoms of amorphous Ge will be approximately C_{3v} by analogy with $GeBr_3H$, for example. Thus the infrared-active stretching and bending modes are nondegenerate (A_1) and doubly degenerate (E), respectively. The integrated absorption for a particular mode of a Ge-H bond will therefore be greater for an assembly of randomly oriented GeH_4 molecules than for the Ge-H bonds in amorphous Ge, in proportion to the ratio of the degeneracies. Using Levin's data for gaseous GeH_4,[23] $(A_{23}+A_{245})/A_{07} = 0.54$ is predicted, where A_{07} is the total integrated intensity of the bond-bending band. The difference from the experimental value of 0.45 reflects the limitations of the model used, but at the same time demonstrates the reasonableness of the approach. The result of such considerations then for the bond-bend-

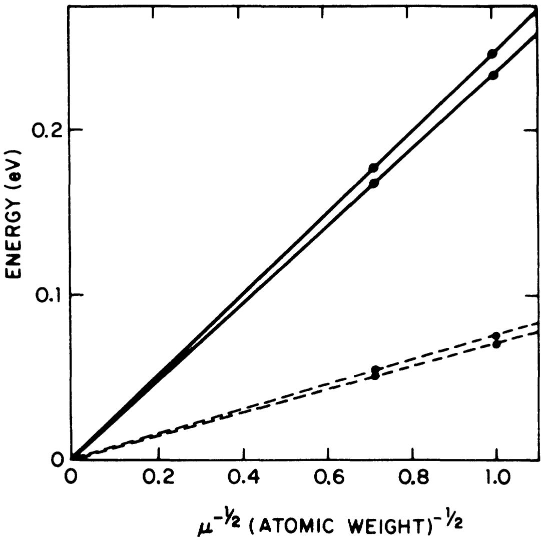

FIG. 5. Oscillator frequency $\hbar\omega_0$ vs the reciprocal square root of the reduced mass for each component of the Ge-H and Ge-D bond-stretching (straight line) and bond-bending (dashed line) vibrational modes.

ing mode, for example, is

$$N(\text{at. }\%) = 0.25 \int_{\text{Absorption band}} \alpha\, d(\hbar\omega) \qquad (3)$$

when α is measured in cm^{-1} and $\hbar\omega$ in eV. The value of N expressed in arbitrary units is used as an accurate measure of the relative hydrogen content of the films. The absolute value of N in at.%, should be regarded as a best estimate of the hydrogen concentration.

The deuterium concentration can be found by noting that

$$I \equiv \frac{1}{\omega_0^2} \int_{\text{Absorption band}} \omega \operatorname{Im}\epsilon(\omega)\, d\omega = 2\pi^2 e^{*2}/k_0 \ .$$

Thus I is a constant for isotopic atoms, a fact which is sometimes called the isotopic sum rule. Levin has demonstrated that it applies well to GeH_4 and GeD_4.[23] Thus for the bond-bending mode of Ge-D,

$$N(\text{at. }\%) = 0.25\left(\frac{0.0170}{0.0515}\right)^2 \int_{\text{Absorption band}} \alpha\, d(\hbar\omega) \ .$$

Again the relative value of N is expected to be more accurate than its absolute value.

The appropriateness of the model described by Eq. (1) is indicated first by Fig. 5, in which $\hbar\omega_0$ is proportional to $\mu^{-1/2}$ for each component of the bending and stretching modes. Parenthetically, this implied identical fractional change of k_0 between either Ge-H or Ge-D bonds in the two configurations suggests that the configurational difference is solely the result of different environments that exist in the Ge matrix, an important point for modeling the hydrogen incorporation. Second, in Fig. 2 a shift of the absorption maximum to lower energy with increasing p_h appears to occur, and gives a value of N, from Eq. (1) for the variation of ω_t, that is consistent with, but considerably less accurate than the basic method described earlier. Both techniques give values of N between 0 and 10 at. % for the materials of this study. In the remainder of this paper, we will describe how the inclusion of hydrogen or deuterium at these levels affects the structure of Ge and its electronic properties. The notation $F(N)$ will commonly be used to identify the films.

B. Structure

In an earlier study, it was shown that the features in the diffraction interference function $\mathcal{F}(s)$ where

$$\mathcal{F}(s) = s\left[I(s)/f^2(s) - 1\right] ,$$

were quantitatively determined at $s \gtrsim 6$ Å^{-1} by the ordering of the first- and second-nearest neighbors alone.[16] This turned out to be almost independent of the density of the material. On the other hand, the intensity of the first peak of $\mathcal{H}(s)$, relative to the second, or alternatively $I(s_1)/I(s_2)$, was extremely sensitive to the ordering of the material outside the tetrahedral subunit and varied dramatically with density[16]: $I(s_1)/I(s_2)$ varied from 0.967 to 1.058 when ρ_0 varied from 4.85 to 5.18 g/cm^3. Thus a comparison of $I(s_1)/I(s_2)$ in different films provides a convenient test of structural variation.[16]

In Fig. 6(a), the measured value of $I(s_1)/I(s_2)$ is plotted for several values of N. The solid line is the average value of $I(s_1)/I(s_2)$ that was obtained in measurements on low-density films ($\rho_0 \approx 4.9$ g/cm^3), prepared by dc sputtering and discussed in detail elsewhere.[16] Therefore to a first approximation the hydrogenated materials of this work at all levels of hydrogenation structurally resemble the low density unhydrogenated material that was studied previously.

At first examination, the density data appear to be at odds with this conclusion. Unhydrogenated material, on the one hand, has a density $\rho_0 = 5.05 \pm 0.05$ g/cm^3 rather than 4.90 ± 0.05 g/cm^3. However, the argon concentration is also higher in these new films by about 3 at. %, and, since the argon atoms reside within the voids of the network,[16] an increase of density $\Delta\rho_0 \approx 0.03 \times (40/72.6) \times 5.0 \approx 0.1$ g/cm^3 is to be expected! At the highest hydrogen concentrations, on the other hand, ρ_0 decreases slightly as shown in Fig. 6(b), although the argon concentration is independent of N. Thus the decoration of the internal void surfaces of unhydrogenated material cannot be the *sole* model of hydrogen incorporation. Ge-H bonds must also exist in regions that would be fully coordinated bulk regions in unhydrogenated material. However, the result-

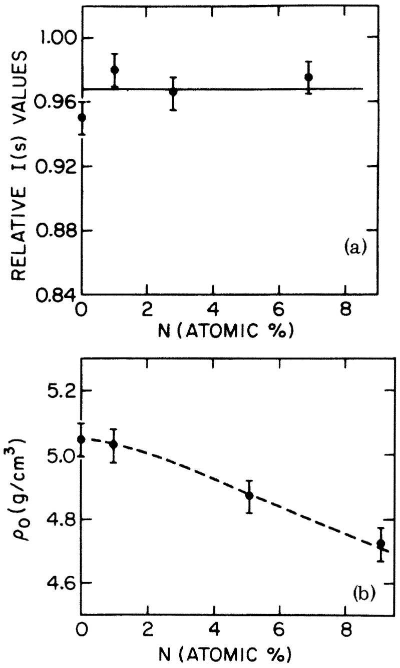

FIG. 6. (a) Ratio of the intensities of the first and second peaks of the diffraction interference function vs the at.% of hydrogen incorporated. (b) Mass density of $Ge_{1-x}H_x$ films vs the at.% of hydrogen incorporated.

ing reorganization of the Ge n-bond neighbors[16] and the introduction of additional voids as opposed to lower density local regions must be negligibly small, since no changes are seen in either $I(s_1)/I(s_2)$ or the total void volume (as measured by the argon concentration). Nevertheless, the topology of the network will be disturbed. A typical case is shown in Fig. 7. The volume v_h associated with the hydrogen atom is approximately N_g^{-1}, where N_g is the number of Ge atoms per unit volume in a fully coordinated network. Larger values of v_h could be obtained but, without introducing dangling bonds, smaller values could not be achieved. The hydrogen atom acts as a Ge chain terminator but as already surmised on the basis of the diffraction data it does not cause any large changes in the distribution of Ge n-bond neighbors.

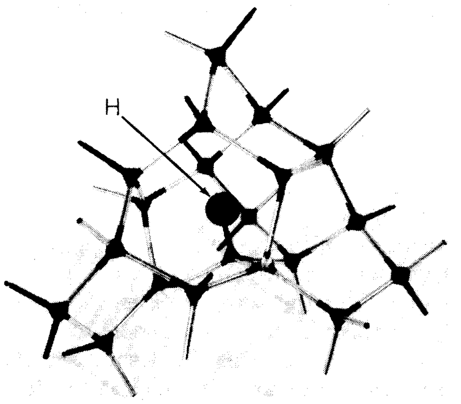

FIG. 7. Example of the network near a bulk-incorporated hydrogen atom.

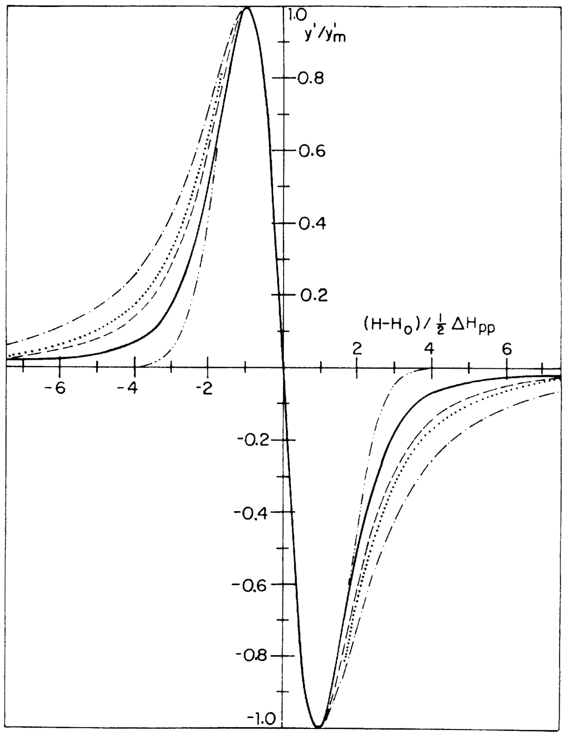

FIG. 8. Normalized first derivative of EPR absorptions vs normalized magnetic field for $Ge_{1-x}H_x$ films: $F(0)$ at 100 K (- - -), $F(0)$ at 300 K (-·-·), and $F(5.1)$ at 100 K (——). Lorentzian (●●●) and Gaussian (··–) line shapes are shown for comparison.

C. Electron paramagnetic resonance

Typical experimental data plotted as y'/y'_m vs $(H-H_0)/\frac{1}{2}\Delta H_{pp}$ are shown in Fig. 8. The resonance occurs at $g = 2.018 \pm 0.002$ at all N, but the line shape and linewidth are a function of both temperature and N. On the one hand, at 100 K and $N = 0$, the line is close to Lorentzian in shape, but it deviates progressively towards a Gaussian line with increasing N. It should be pointed out that the Gaussian and Lorentzian lines, shown for comparison in Fig. 8, have undergone the same small baseline correction procedure as the experimental data. This process has no effect near the center of the resonance, but forces the first derivative to converge to zero at $|(H-H_0)/\frac{1}{2}\Delta H_{pp}| \geq 20$. On the other hand, an increase in temperature at $N = 0$ produces a change of line shape in the opposite direction.

The temperature dependence of ΔH_{pp} is shown in Fig. 9 for a selection of unhydrogenated and hydrogenated materials and the reproducibility of the results is demonstrated by data points for two different $N = 0$ samples. There is a low-temperature regime for all N in which ΔH_{pp} is independent of temperature but increases with N from 31.4 G for $N = 0$ to 38 G for $N = 5.1$. The transition to a temperature-dependent regime occurs at progressively higher temperatures with increasing N. Indeed, for $N > 3$, ΔH_{pp} is temperature independent within the range of measurement. For comparison, in Fig. 10, the temperature dependence of ΔH_{pp} for an $N = 0$ film before and after an anneal at 320 °C for 6 h is shown. As with hydrogenation, the temperature-dependent regime is shifted to higher temperatures but in contrast with hydrogenation ΔH_{pp} in the low-temperature regime is decreased. It is apparent from an examination of Fig. 9 (and later in Fig. 12), that hydrogenated and deuterated material cannot be differentiated in these EPR experiments indicating that effects of the hydrogen nuclear spins are minimal. Thus the changes observed with increasing N and annealing in ΔH_{pp} are solely associated with the induced changes in the interactions between the electrons in singly occupied electronic states. Correlations between these paramagnetic resonance effects and other electronic properties might therefore be expected.

In Fig. 11, the N dependence of l, the line-shape factor, is shown at temperatures of 100 and 300 K. The reduction of l with N in the low-temperature regime is relatively small, but is much larger at 300 K. The difference is readily traced to the

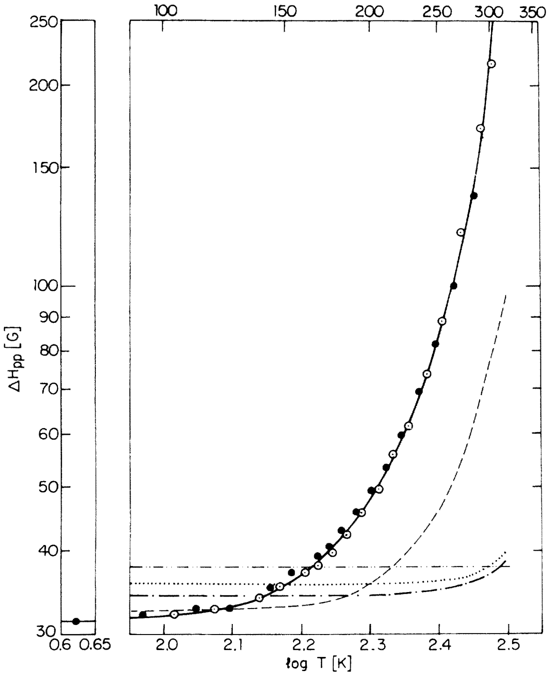

FIG. 9. Linewidth of the first derivative of EPR absorptions vs logarithmic temperature for $Ge_{1-x}H_x$ films: $F(0)$ (——), $F(1)$ (– – –), $F(2.8)$ (-··-·), and $F(5.1)$ (-··), and for $Ge_{1-x}D_x$ film: $F(3)$ (• • •). Data (○○○) and (●●●) illustrate the reproducibility of 2 $F(0)$ films.

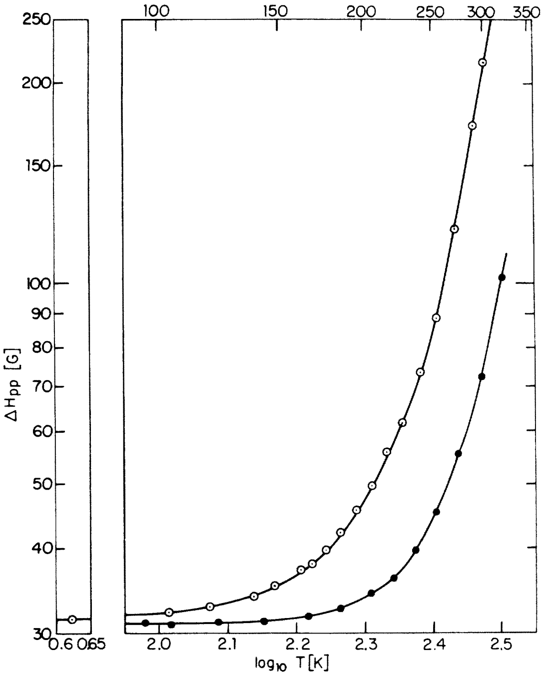

FIG. 10. Linewidth of the first derivative of EPR absorptions vs logarithmic temperature for Ge film $F(0)$ before (○○○) and after (●●●) a 320 °C anneal for 6 h.

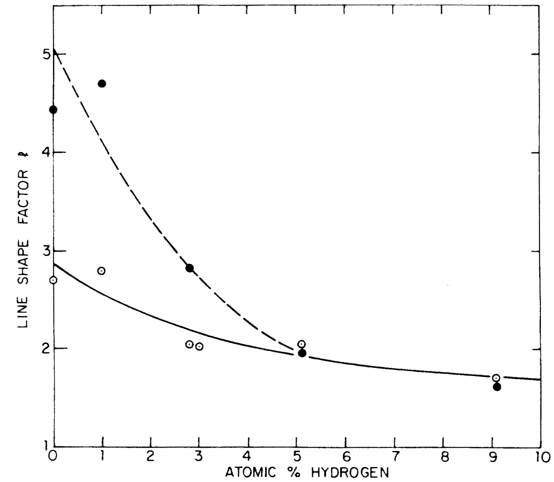

FIG. 11. Line-shape factor $l = A/(y_m'/\Delta H_{pp}^2)$ measured at 100 K (○○○) and 300 K (●●●) vs the at.% of hydrogen incorporated.

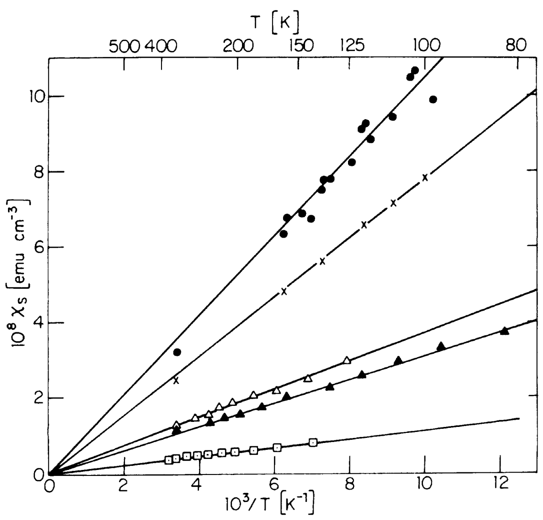

FIG. 12. Magnetic susceptibility per unit volume vs reciprocal temperature for $Ge_{1-x}H_x$ films: $F(0)$ (●●●), $F(1)$ (×××), $F(2.8)$ (△△△), and $F(5.1)$ (□□□), and for $Ge_{1-x}D_x$ film: $F(3)$ (▲▲▲).

large temperature dependence of l in regions where ΔH_{pp} varies rapidly with temperature. For example, in unhydrogenated material, for which the temperature dependence of ΔH_{pp} is largest, $l = 2.71$ at 100 K and $l = 4.43$ at 300 K. It is worth emphasizing again that the failure to include these variations would result in considerable systematic errors in the determination of $\chi_0(T)$. At values of N greater than about 3, l and, parenthetically, ΔH_{pp} are temperature independent within experimental error in the range examined.

The susceptibility per unit volume derived from these data is plotted versus reciprocal temperature in Fig. 12. Between 100 and 350 K, each sample shows Curie behavior, from which a well-defined spin density can be obtained. Clearly, the spin density decreases markedly with increasing N, but the decrease is less rapid at large N than at small N. In fact, the variation with N is much the same as that of A_{23}, a correlation that will be discussed in detail later.

D. Absorption edge and refractive index

The absorption edge of unhydrogenated amorphous Ge has been the subject of many studies and much controversy.[19] It is agreed that in the range 10^3 cm$^{-1} \lesssim \alpha \lesssim 10^4$ cm^{-1} its position and to a lesser extent its shape depend on preparation conditions. However, the sharpness of the onset of absorption below $\alpha \approx 10^3$ cm^{-1} is contested. On the one hand, Donovan, Spicer, Bennett, and Ashley (DSBA) have claimed that in optimally prepared evaporated films a "sharp" edge occurs for which α decreases from 10^3 to 10 cm^{-1} in about 0.05 eV.[29] On the other hand, several workers studying similar material have observed a "shallow" edge in which α decreases from 10^3 to 10^2 cm^{-1} in about 0.25 eV. Subsequently, Connell and Lewis[19] reanalyzed DSBA's original data and Donovan's later data[30] to demonstrate that they are at the most not inconsistent with a "shallow" edge when random and systematic errors in α, determined from films with thicknesses of order 2000 Å, are correctly included. At the least, a "sharp" edge is necessarily masked by their experimental errors. In the present study α was determined to ± 30 cm^{-1}, so that a "shallow" edge will be clearly distinguished from a "sharp" edge.

In Fig. 13, the absorption edge of sputtered unhydrogenated material ($T_s = 25$ °C) is shown for $\hbar\omega \lesssim 0.6$ eV. Above $\alpha \approx 30$ cm^{-1}, the absorption edge is approximately exponentially dependent on photon energy, although it appears that the absorption rises more rapidly at the lowest energies. However, the edge is not "sharp" at any energy. When N is increased at fixed T_s and fixed T_a, the absorption at a given photon energy decreases as shown in Figs. 13 and 14. However, for all values of N the absorption between 2×10^2 and 5×10^3 cm^{-1} can be parameterized as $\alpha(\omega, N) = \alpha_0(N)\exp[\hbar\omega/E_s(N)]$. In Fig. 15, $\alpha_0(N)$ is plotted vs $E_s(N)$. It appears that $T_a = 250$ °C and $T_s = 250$ °C films of equal N are quite similar but differ significantly from their $T_s = 25$ °C counterparts. In contrast, the effect of increasing N appears to be independent of T_s and T_a as might reasonably be expected.

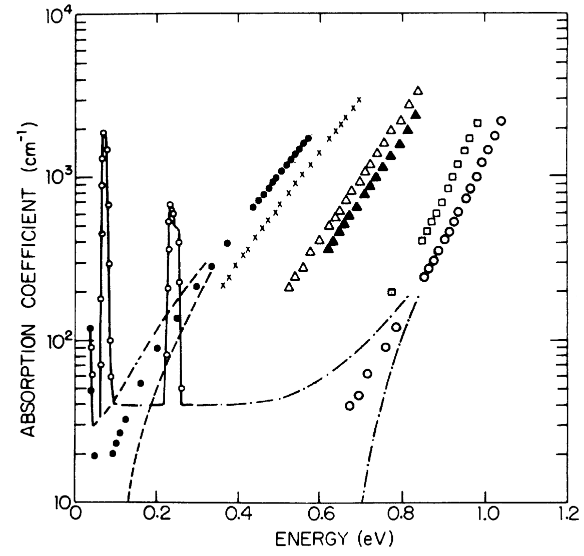

FIG. 13. Absorption coefficient vs photon energy for $Ge_{1-x}H_x$ films: $F(0)$ (●●●), $F(1)$ (×××), $F(2.8)$ (△△△), $F(3.0)$ (▲▲▲), $F(5.1)$ (□□□), and $F(8)$ (○○○). Error estimates on $F(0)$ data (- - -) and $F(8)$ data (-··-·) are shown.

At $N \gtrsim 5$ at.% (or $p_h \gtrsim 10 \times 10^{-4}$ Torr), the optical properties investigated approach asymptotic values that depend only on T_s or T_a. The N dependence of E_α, the photon energy at which $\alpha = 10^3$ cm^{-1}, and the refractive index measured at a photon energy of 0.125 eV, both shown in Fig. 16 for $T_s = 25$ °C films, are typical examples. Thus it appears that these electronic properties are not modified by hydrogen incorporated into sites that produce A_{245}, but asymptote with N in much the same way as A_{23}. Furthermore, different asymptotic values are reached upon hydrogen incorporation into samples with different thermal histories as might be deduced from Fig. 15, suggesting the possibility of separable contributions to the changes of the electronic density of states from dangling bond removal and network reorganization.

It is appropriate to compare these new data with those of Connell *et al.*[18] In that study amorphous Ge prepared by dc sputtering onto substrates held at 350 °C, had an absorption edge and refractive index that were comparable to those of as-prepared $F(3.5)$. In contrast, the density and coordination number of the material were 5.18 ± 0.03 and 3.91 ± 0.1, respectively, significantly greater than those of $F(3.5)$. Thus, both an increase of T_s and hydrogen incorporation at low T_s though producing different structural changes result in similar modifications to the specific optical properties investigated. The present results would suggest, however, that still higher-density unhydrogenated material could be made, in which the edge and refractive index were more comparable to those of annealed $F(8)$, for example, and the coordination number was presumably closer to 4.0. Of course, the structural changes during the annealing of $F(8)$ might be quantitatively different from the network relaxation occurring in fully coordinated material, but the qualitative aspects of this argument should certainly be true.

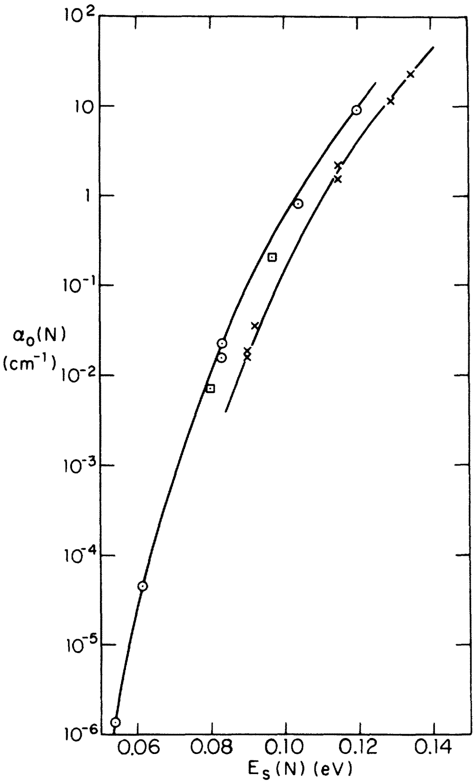

FIG. 15. $\alpha_0(N)$ vs $E_s(N)$ for $Ge_{1-x}H_x$ films with $T_s = 25$ °C before (× × ×) and after anneal at 250 °C for 1 h (○○○) and for $Ge_{1-x}H_x$ films with $T_s = 250$ °C (□□□). Absorption coefficient has been fitted to $\alpha(\omega, N) = \alpha_0(N) e^{\hbar\omega / E_s(N)}$.

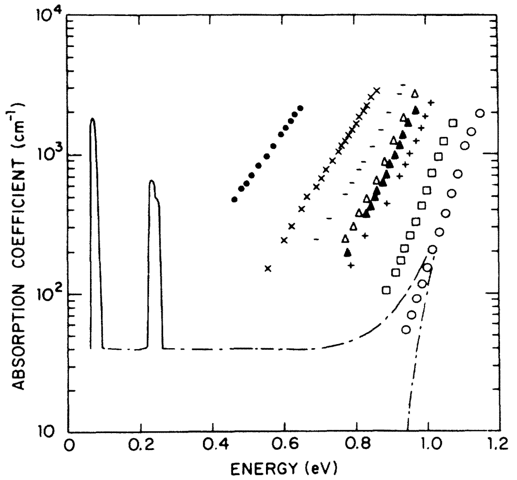

FIG. 14. Absorption coefficient vs photon energy for $Ge_{1-x}H_x$ films: $F(0)$ (●●●), $F(1)$ (×××), $F(2.8)$ (△△△), $F(3.0)$ (▲▲▲), $F(5.1)$ (□□□), and $F(8)$ (○○○), after a 250 °C anneal for 1 h and for $Ge_{1-x}H_x$ films: $F(\approx 1)$ (– – –) and $F(4.2)$ (+ + +) produced at $T_s = 250$ °C. Error estimates on $F(8)$ data (–•–•) are shown.

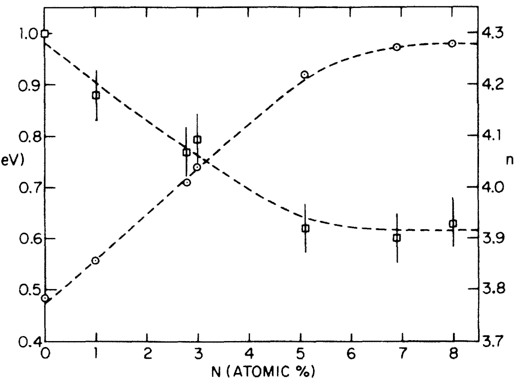

FIG. 16. E_α, the energy at which the absorption coefficient is 1000 cm^{-1} (○○○), and n, the refractive index measured at a photon energy of 0.125 eV (□□□) vs the at.% of hydrogen incorporated.

IV. DISCUSSION

A. Structural aspects of hydrogen incorporation

It was argued earlier from structural data that hydrogenation occurs not only through absorption to the surfaces of voids but also through incorporation of isolated hydrogen atoms in the bulk. It is therefore imperative to find a measurable property that can differentiate between hydrogen atoms in the two environments before the trends in the electronic properties can be understood quantitatively. But what are the hydrogen concentrations involved in the two cases? On the one hand, from the coordination number of unhydrogenated material of 3.8 ± 0.1,[16] the maximum number of hydrogen atoms that can bond on void surfaces, N_{s0}, is expected to be $N_{s0}=5\pm2.5$ at. %, if one hydrogen atom pairs with each dangling bond. On the other hand, the maximum number of hydrogen atoms that can bond in the bulk, N_{b0}, is set solely by the requirement of material cohesion. Each Ge atom must therefore lie on at least one infinite chain of Ge atoms, which using bond percolation theory requires that each Ge atom must be connected with a minimum of 2.5 other Ge atoms.[31] In different words, each Ge atom can be associated with a maximum of 1.5 hydrogen atoms in cohesive material. Thus, a maximum of approximately $N_{b0}=60$ at. % of hydrogen can be incorporated in the bulk.

The ratio of surface to bulk sites may also be calculated directly from structural data. If a void is considered to be equivalent to the removal of a cluster of n fully bonded atoms from a fully coordinated network, then it was shown experimentally that the fraction f of the bonds that the n atoms made with atoms outside the cluster, i.e., with atoms on the surface of the void rather than with atoms within the cluster, is $f=0.6\pm0.2$.[16] Furthermore, the voids are typically 5 Å across with centers 10 Å apart.[16] (A void could typically contain five atoms and, in this case, would be 7.5 Å across.) Thus the ratio $N_{s0}/N_{b0}=(0.6\pm0.2)$ times the void-volume to bulk-volume ratio, $=0.085\pm0.02$, and compares favorably with $N_{s0}/N_{b0}=\frac{5}{60}=0.083$ that was derived above. In fact, a much poorer agreement would be quite satisfactory, since the ratio of the void volume to bulk volume is sensitive to the assumed shape and precise size of the voids.

Such concentrations of hydrogen atoms would be clearly detectable through the vibrational spectra of the Ge-H bond. But does this technique differentiate between the two environments? Becker and Gobeli observed that the Si-H bond-stretching vibration occurred at a smaller photon energy for hydrogen atoms on crystalline Si surfaces than for isolated hydrogen atoms in the bulk crystal, in the ratio 0.96 : 1.[32] A comparable effect would be expected in the present case. Associating the 0.232-eV bond-stretching mode with void surface sites and the 0.245-eV bond-stretching mode with bulk sites of amorphous Ge allows a ratio of 0.94 : 1 to be calculated. Similarly, a ratio of 0.96 : 1 is obtained for amorphous Si. Both of these are in excellent agreement with the crystalline Si result. Further confirmation of this interpretation is derived from the magnitude and dependence on p_h of either A_{23} or A_{245}. A_{23} reaches an asymptote A_{symp} corresponding to the incorporation of about 3.5 at. % of hydrogen on void surfaces, in excellent agreement with the earlier prediction for N_{s0}. In future it will be assumed that A_{symp} and N_{s0} are equivalent. In contrast A_{245} continues to rise in the range of investigation, as should be expected for levels of hydrogen incorporation that are very much less than $N_{b0}=60$ at. %.

Correlation of different structural and electronic properties now becomes possible. First, if it is assumed that the electron spin density n_s obtained in EPR measurements is proportional to the number of dangling bonds not bonded to hydrogen atoms, then

$$n_s=B(N_{s0}-A_{23})\ ,$$

where A_{23} is expressed in at.% using the results of Sec. IIIA, and B gives the number of spins per "dangling bond." In Fig. 17, n_s is plotted vs A_{23}. The slope indicates that a spin is measured only for about every 100 electrons on the internal sur-

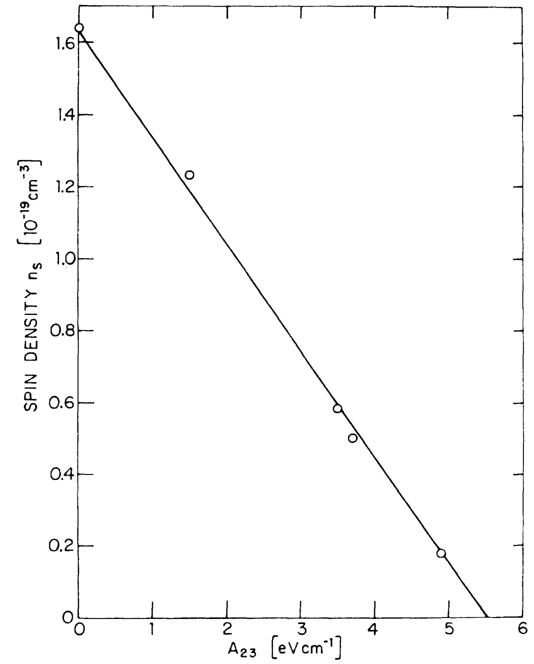

FIG. 17. Spin density vs the integrated intensity of the 0.23-eV absorption.

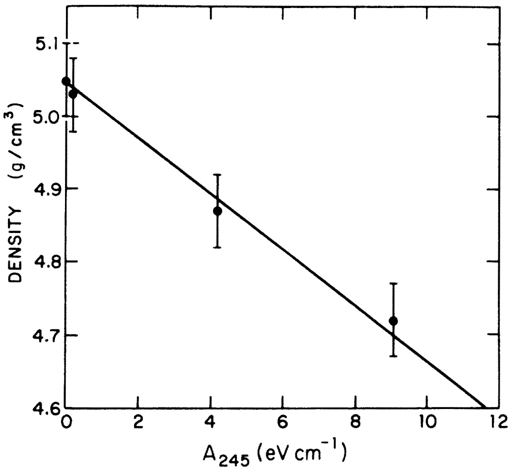

FIG. 18. Mass density vs the integrated intensity of the 0.245-eV absorption.

faces in unhydrogenated material. Since the voids are typically 5 Å across, there are of order 10–20 dangling bonds on each void surface or one spin in 5–10 voids. Thus, the spins are, on average, separated by about 20 Å. This separation is satisfactorily consistent with the estimate of about 40 Å that is obtained from the spin density directly. We will return to this subject in Sec. IV C.

Second, if a volume v_h is associated with each hydrogen atom in the bulk, a correlation between the density of the material and A_{245} is obtained. Namely, for small values of A_{245},

$$\rho = \rho_0 (1 - \tfrac{1}{100} A_{245} N_g \langle v_h \rangle) ,$$

where $\langle v_h \rangle$ is the average value of v_h, N_g is the number of Ge atoms per unit volume in a fully coordinated network, ρ_0 is the density of the unhydrogenated material, and A_{245} is measured in at.%. In Fig. 18 the linear dependence of ρ on A_{245} is demonstrated and these data show that $\langle v_h \rangle = 32$ Å^3. Thus $\langle v_h \rangle$ is approximately equal to the volume per atom in the fully coordinated network of 24 Å^3, which together with the earlier model study, indicates that $v_h \approx \langle v_h \rangle$ at all bulk sites and extends the more general structural arguments of Sec. III B.

The vibrational spectra thus provide a workable scale of hydrogen incorporation into the two types of environment and together with density data and simple model studies provide insight into the local structure of the bulk sites. At the same time, it should be noted that the bending and stretching modes of Ge-H bonds have been observed in electrolytically deposited amorphous Ge,[26] and in Ge prepared at $T_s \approx 300$ K by the rf decomposition of GeH_4.[27] In these cases, however, the stretching mode is a symmetric singlet and occurs at 0.23 eV. We conclude then that in these materials hydrogen lies only on void surfaces. For electrolytic material the process of deposition would appear to lead to the same conclusion inasmuch as hydrogen atoms are released at the electrode only upon the deposition of Ge atoms. Voids are thus necessarily heavily coated with hydrogen.

B. Logistics of hydrogen incorporation

Section IV A has provided a framework on which the discussion of the trends in the experimental optical and transport results can be based. However, it is appropriate to ask how hydrogen incorporation onto the void surfaces and into the bulk regions occurs. The fact that $A_{23} \sim p_h$ and $A_{245} \sim p_h^2$ at small p_h indicates that hydrogenation of the two types of sites does not occur in qualitatively the same way but at different rates. Rather, it appears that the hydrogenation of bulk sites possibly depends on the hydrogenation of the internal surface sites. In the early part of this investigation, a model in which the hydrogenation of an A_{23} void site generated in the surrounding void sites a number of A_{245} sites were considered, but it was not able to explain quantitatively the experimental data. In fact, it could not explain the data on $Ge_{1-x}H_{0.5x}D_{0.5x}$ qualitatively, since it did not predict that the spectra of this material was a linear superposition of the $Ge_{1-x}H_x$ and $Ge_{1-x}D_x$ spectra. In contrast, a model of nucleation and growth of hydrogenated areas on the instantaneous growth surface has proved to be quite satisfactory and demonstrates in a physical way the origin of hydrogenation on internal surfaces and in bulk regions.

Amorphous Ge, sputtered at $T_s \approx 25$ °C, contains voids typically 5 Å across with centers 10 Å apart.[16] The instantaneous growth surface during sputtering in pure argon will thus be as sketched in Fig. 19. The valleys are nascent voids and are

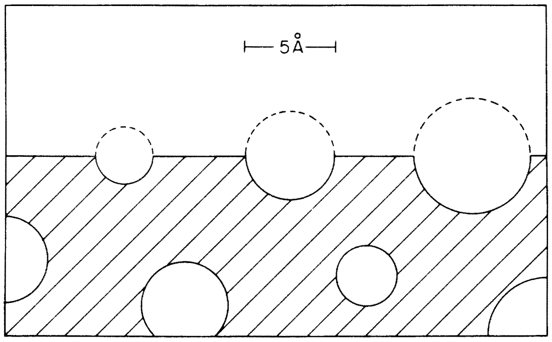

FIG. 19. Stylized model of an instantaneous growth surface of a film during deposition. Voids are typically 5 Å across the separated by 5 Å.

typically 1–3 monolayers deep. Since no further deposition of Ge atoms occurs in them during the formation of the film, the arrival rate of Ge atoms in them is zero and the surface mobility of Ge adatoms on the plateaus is sufficiently small to prevent diffusion into them in the time required to deposit several monolayers. According to Shevchik,[33] the arrival rate near nascent voids is made small by the variations in the surface field that result from the surface topography.[33] What happens then if hydrogen is now added to the argon? The chance of reactive sputtering occurring is unlikely, since the chance of collisions between Ge and H atoms, the chance that such collisions result in Ge-H bonds, and the stability of such bonds in the rf plasma are all small under the present experimental conditions. Hydrogen incorporation must occur through the hydrogen atoms created by the plasma that impinge on the growth surface. It is assumed here that the arrival rate depends linearly on the hydrogen partial pressure p_h.

The hydrogen adatoms diffuse rapidly across the growth surface on arrival because of their higher incident thermal velocity and as a result lose the competition for bonding sites on the plateaus to the Ge atoms that bond at their point of arrival. The incipient voids, on the other hand, act as nucleation centers for hydrogen adsorption in the same way as steps on metallic surfaces.[34] The enhancement of adsorption in the valleys over the plateaus is particularly exaggerated in the present case, however, by the additional element of competition for bonding sites on the plateaus. Ge-H bonds are thus formed preferentially on void surfaces, although at high p_h the formation of Ge-H bonds on plateaus sites by diffusion out of the nascent voids should be expected. In the following this model is given a mathematical foundation.

Consider the instantaneous growth surface of Fig. 19. It has N_1 valley sites and N_2 plateau sites. At a given time, n_1 valley sites and n_2 plateau sites are permanently bonded by hydrogen atoms. If h is the number of hydrogen atoms on the surface capable of bonding per unit time per unit area, i.e., $h \propto p_h N_1$, then the probability of capture of a hydrogen atom in a valley is the product of the probability of finding an empty valley site times the probability, C_1, of capture at an empty valley site

$$\frac{dn_1}{dh} = \left(\frac{N_1 - n_1}{N_1}\right) C_1 \ .$$

Similarly, the probability of capture of a hydrogen atom on a plateau is the product of the probability of diffusing out of a valley times the probability of finding an empty plateau site times the probability, C_2, of capture at the empty site

$$\frac{dn_2}{dh} = \left(1 - C_1 \frac{N_1 - n_1}{N_1}\right) \frac{N_2 - n_2}{N_2} C_2 \quad ,$$

where C_2 is approximately equal to or somewhat less than C_1. In the latter case, C_2 would include a term to represent the competition from the Ge atoms that arrive on the plateaus. It is convenient to put $h = (C'/C_1)\, p_h N_1$ and write the solutions for n_1 and n_2 as

$$n_1 = N_1 (1 - e^{-C' p_h})$$

$$n_2 = N_2 \left\{ 1 - \exp\left(\frac{C_2 N_1}{N_2}\right) \times \exp\left[- \frac{C_2 N_1}{N_2} \left(\frac{C' p_h}{C_1} + \exp(-C' p_h) \right)\right]\right\} .$$

Integration over the deposition time finally gives

$$A_{23} = N_{s0} (1 - e^{-C' p_h}) \ ,$$

$$A_{245} = N_{b0} \left\{ 1 - \exp\left(\frac{C_2 N_{s0}}{N_{b0}}\right) \times \exp\left[- \frac{C_2 N_{s0}}{N_{b0}} \left(\frac{C' p_h}{C_1} + \exp(-C' p_h) \right)\right]\right\} , \quad (5)$$

where A_{23} and A_{245} are again expressed in at.%. It is of interest to examine the behavior of A_{23} and A_{245} in the limit of N_{s0} tending to zero, since when T_s is increased particularly above some critical value a reduction of N_{s0} is expected.[10] For values of p_h at which $A_{23} \approx A_{245}$, $e^{-C' p_h} \approx 0$ and we get

$$\lim_{N_{s0} \to 0} A_{23} = N_{s0} \ ,$$

$$\lim_{N_{s0} \to 0} A_{245} = C_2 N_{s0} (C' p_h / C_1 - 1) \ ,$$

$$\lim_{N_{s0} \to 0} (A_{23} + A_{245}) = N_{s0} [1 + C_2 (C' p_h / C - 1)] \ ,$$

$$\lim_{N_{s0} \to 0} A_{245} / A_{23} = C_2 (C' p_h / C_1 - 1) \ .$$

Thus A_{23}, A_{245}, and $A_{23} + A_{245}$ tend to zero as N_{s0} but the ratio, A_{245}/A_{23}, is independent of N_{s0}. It is likely that as N_{s0} tends to zero in an actual case, some deviations from these predictions will be observed, i.e., A_{245} will probably remain finite, but this is not expected to be a problem for the materials investigated in this study. These features are characteristic of the model of nucleation and growth postulated here and tend to differentiate it from other models of hydrogenation.

Finally, the electron spin density n_s can be written down for comparison with experiment

$$n_s = B(N_{s0} - A_{23}) = B N_{s0} \, e^{-C' p_h} \ .$$

The value of C' is predetermined by the vibrational data making the EPR results a convenient cross-check of the model parameters.

In Fig. 4, A_{23} and A_{245} of $T_s = 25$ °C films plotted vs p_h are fit by Eqs. (4) and (5), respectively. It was assumed for simplicity that C_1 is unity. The fitted expressions are then

$$A_{23}(\mathrm{eV\,cm^{-1}}) = 5.8[1 - e^{-3820\,p_h}] ,$$

$$A_{245}(\mathrm{eV\,cm^{-1}}) = 80(1 - 1.06 \exp\{-0.058[3820\,p_h + \exp(-3820\,p_h)]\}) ,$$

giving

$$N_{s0} = 3.5 \text{ at. \%}, \quad N_{b0} = 45.0 \text{ at. \%} ;$$

$$C_2 = 0.8 , \quad C' = 3820 \times 10^4 \text{ Torr}^{-1} \quad \text{with } p_h \text{ in Torr.}$$

The value of C' has no physical significance, but the values of the other parameters are extremely important for the physical meaningfulness of the model. C_2 was earlier argued to be approximately equal to or slightly less than C_1. This is evidently true and $C_1 \approx C_2 \approx 1$ indicates that hydrogen bonds whenever a site is available after nucleation in either valleys or plateaus. The values of N_{s0}, N_{b0}, and $N_{s0}/N_{b0} = 0.075$ agree tolerably well with those derived solely from structural considerations in Sec. IV A. Furthermore, the agreement between experiment and the predicted dependence of n_s on $e^{-3820\,p_h}$ is excellent, demonstrating the internal consistency of the model. Finally as explained in Sec. III A the value of $A_{23} + A_{245}$ at a large p_h is smaller in $T_s = 250$ °C material than in $T_s = 25$ °C material, yet A_{23}/A_{245} is unchanged. This is a direct prediction of the model, if N_{s0} is reduced on the high-temperature growth surface.

We believe that the foregoing results establish quantitatively the validity of the model for hydrogen incorporation and lend further support for the interpretation of the vibrational spectrum.

C. Electronic properties

In discussing the effect of hydrogenation on the electronic states of the amorphous material two cases must be distinguished. In the first case, the hydrogenation of N_{s0} states, an effect that parallels the hydrogenation of crystalline surface states will occur. For example, Ibach and Rowe[35] have investigated the hydrogenation of several crystalline Si surfaces using photoemission and energy-loss spectroscopy.[35] Independent of the crystallographic face studied, they found that hydrogen bonded by "dangling bonds" shifted states from near the valence-band edge to about 6 eV into the valence band. Moreover, the states associated with back bonds, which occur deeper in the valence band, disappeared simultaneously indicating that hydrogenation redistributes the charge density in the back bonds towards a distribution more similar to that of bulk silicon. Thus we expect that hydrogenation of N_{s0} states will lead to a decrease in absorption at photon energies that are less than the gap in fully coordinated material. Moreover, the shift of states from the upper valence-band edge to deep in the valence band will also cause a reduction in refractive index.

In the second case, the hydrogenation of N_{b0} states, dangling bonds are not replaced by Ge-H bonds. In fact, the bond strengths of the Ge-H and Ge-Ge bonds are comparable, 76 and 65 kcal/mole, respectively,[36] and to a first approximation it may be assumed that neither the absorption near the gap nor the refractive index will be affected.

It follows then that the absorption edge and refractive index should asymptote with increasing p_h in the same way as A_{23}. This correlation was noted earlier and demonstrated in Fig. 16. The asymptotic values of the refractive index and the energy at which $\alpha = 10^3$ cm^{-1} are 3.92 ± 0.05 and 1.0 ± 0.02 eV, respectively, in unannealed material, and 3.88 ± 0.05 and 1.1 ± 0.02 eV, respectively, in annealed material. The difference between these two sets of data is caused by the structural relaxation process that is generated by annealing. However, in fully hydrogenated material this relaxation process cannot include the removal of dangling bonds. Thus the results suggest that the optical gap in fully coordinated amorphous Ge lies in a region near 1 eV, defined at low energies by the absorption edge of fully hydrogenated unannealed material and at high energies by the absorption edge of fully hydrogenated annealed material. This region is shown in Fig. 20. For comparison, Theye's data on a 500-Å thick anneal stable evaporated amorphous Ge film is shown.[37] Annealing has evidently produced material with an absorption edge that is close to the lower bound for full coordination. In contrast, an examination of other absorption edges reported in the literature for so-called "void free" amorphous Ge,[11] indicates that these materials still contain a considerable number of internal surface states.

A quantitative relationship between optical absorption in the gap of partially coordinated material and the internal surface states was first suggested by Brodsky and Kaplan.[38] Arguing that the density of states $\rho(E)$ in this region could be approximately written

$$\rho(E) \approx \rho_0(E) + \rho_s(E) n_s ,$$

where $\rho_0(E)$ is the bulk density of states at energy E, $\rho_s(E)$ is proportional to the surface density of states per dangling bond at energy E, and n_s (the spin density) is a measure of the number density of dangling bonds; they showed that the absorption coefficient at a photon energy $\hbar\omega$ was

$$\alpha(\omega) \approx a_0(\omega) + a_1(\omega) n_s + a_2(\omega) n_s^2 ,$$

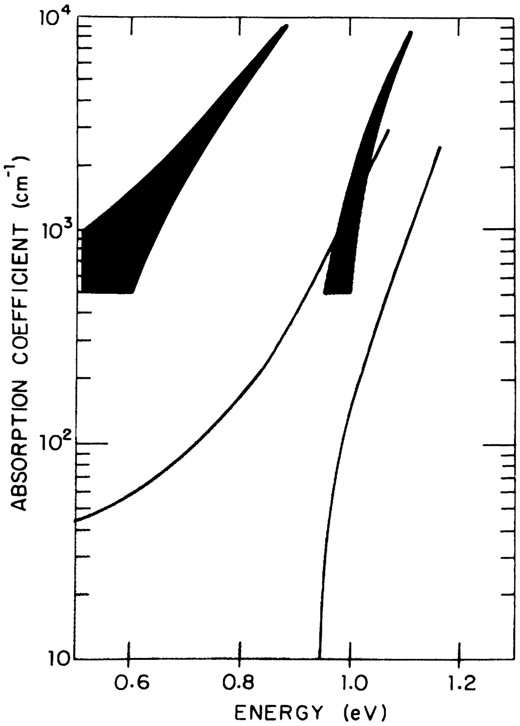

FIG. 20. Absorption edge of fully coordinated amorphous germanium is estimated to occur within the shaded region. For comparison Theye's data on thin evaporated films are shown in black: the edge in as-prepared material is at low energies and the edge in anneal stable material is at high energies.

where a_0, a_1, and a_2 are constant coefficients at fixed $\hbar\omega$. When transitions between surface and bulk states could be neglected, i.e., at small enough $\hbar\omega$ the expression for $\alpha(\omega)$ reduced to

$$\alpha(\omega) \sim a_2(\omega) n_s^2 .$$

In the present work, a direct measure of the number of dangling bonds is available through $(N_{s0} - A_{23})$. Thus

$$\alpha(\omega) \sim a_2(\omega)(N_{s0} - A_{23})^2$$

is expected for a limited range of photon energy. Examination of the data for unannealed material in Fig. 13 indicates that this is indeed observed for $\hbar\omega \lesssim 0.6$ eV, a result that is entirely consistent with our earlier estimate for the gap in fully bonded material. Furthermore, it would appear that the filled and empty surface states span a large fraction of the energy gap, in agreement with our earlier work[10] and recent work by Jones *et al.*[39] and consistent with the calculations of crystalline surface states by Appelbaum and Hamann.[40]

It is appropriate at this juncture to return to the question of the relationship between the number of dangling bonds and the small spin density. There are it appears at least two possible explanations: first, by a surface reconstruction, in which almost all the dangling bonds cross-link to form weak molecular bonds and the spin signal arises from the small number of unpaired electrons that remain; second, by bipolaron formation in which almost half the dangling bond sites have two antiparallel spins and the others have none.[41] Both of these can explain the observation of one spin for each 100 dangling bonds, and it is not clear at the moment which explanation is to be preferred. It is clear that all of them could imply a relationship between spin resonance and conductivity data. For example, the temperature dependence of ΔH_{pp} could represent the lifetime broadening of the singly occupied states that sets in when the probability of electron hopping between localized states becomes significant.[42] In fact, as might be expected for this mechanism it is found that $\Delta H_{pp}(T) \approx \Delta H_{pp}(0) + \text{const} \times \sigma(T)$, where $\sigma(T)$ is the conductivity in the nonactivated region.[12,14] Unfortunately, a more detailed test of this approach is at present complicated by the temperature and hydrogen concentration dependence of the line shape. However, this aspect of the investigation will be discussed in a future paper.

We earlier argued that the spins were separated on average by about 20 Å in unhydrogenated material containing 10^{19} spins/cm^3. This is comparable with the estimate of 10 Å of Paesler *et al.* that was made by assuming that the temperature-independent component of the linewidth arose solely from the dipolar interaction of 10^{20} spins/cm^3.[43] This comparison, however, is not entirely satisfactory for a number of reasons. For example, dipolar broadening decreases with increasing spin separation, yet with hydrogenation at 100 K ΔH_{pp} increases from 32.0 to 40.4 G and $\Delta H_{1/2}$, estimated from numerically integrated data, is constant at 52.7 ± 2 G. Similarly, amorphous Si with a spin density close to that of amorphous Ge has a linewidth narrower by a factor of 5.[44] Evidently additional broadening or narrowing mechanisms must be evoked to resolve these conflicts. The discussion of these problems will be considered in a future paper.

V. SUMMARY

A method of hydrogenating the surfaces of voids has been developed for systematically studying the variation of the electronic properties of gap states in sputtered amorphous Ge with the number of dangling bonds, thus allowing the effects of network reorganization during annealing, for example, to be separately examined.

The role of incorporated hydrogen was examined by the correlation of x-ray diffraction, electron paramagnetic resonance, and optical spectroscopy.

Both the bending and stretching modes of the Ge-H bond are doublets; the lower-energy feature of the doublet is associated with hydrogen atoms residing on the surfaces of voids, and the higher-energy feature is associated with hydrogen atoms residing in the bulk. The variation of the distribution of hydrogen between these two sites with total incorporation sets stringent requirements for a model of the reaction at the gas-solid interface during sputtering. The model developed in which the presence of surface irregularities is central to the rate of reaction, successfully predicts the correlations between the oscillator strengths of the vibrational modes and the electron-spin and mass densities. It is now intriguing to know whether the model will also describe the logistics of reaction at other gas-solid interfaces.

The origin of the states in the gap of partially coordinated amorphous Ge was traced to the dangling bonds on void surfaces. These states span a large fraction of the energy gap of partially coordinated material, to the extent that transitions between them completely determine the optical absorption below photon energies of about 0.6 eV. Optical absorption across the band gap itself in fully coordinated material does not occur until about 1 eV. Comparison of the present data with published optical spectra of so-called "void free" amorphous Ge indicates that, in general, a considerable number of dangling bonds still remain in the latter.

The electron paramagnetic resonance spectra have several complicating features: the spin density is much smaller than the dangling bond density, indicating that electrons most often pair to form weak molecular bonds or bipolarons on the void surfaces; the increase in linewidth with hydrogenation yet a decrease with annealing in the temperature-independent regime is in conflict with a pure dipolar broadening mechanism and suggests a sensitivity to local structural variations; and the temperature dependence of the linewidth, which results in a line-shape variation that can mask the Curie-like behavior, appears to be correlated with the temperature dependence of the nonactivated conductivity. These features will be the subject of a future publication.

ACKNOWLEDGMENTS

We thank A. J. Lewis for his help throughout this work and W. Paul for many suggestions and discussions. We also acknowledge R. J. Temkin and T. D. Moustakas. Finally, we thank D. MacLeod and L. DeFeo for their technical assistance.

---

*Work supported by the National Science Foundation (Contracts DMR-7203020 and GH-38830 X) and the Joint Services Electronic Program (Contract N00014-75-C-0648).

[1] For a review see G. A. N. Connell [Phys. Status Solidi B 69, 9 (1975)].

[2] N. F. Mott, Adv. Phys. 16, 49 (1967); Philos. Mag. 17, 1259 (1968).

[3] M. L. Cohen, in *Proceedings of the Tenth International Conference on the Physics of Semiconductors*, edited by S. P. Keller, J. C. Hensel, and F. Stern (U.S. A.E.C., Cambridge, 1970), p. 645; E. N. Economou, M. H. Cohen, K. F. Freed, and E. S. Kirkpatrick, in *Amorphous and Liquid Semiconductors*, edited by J. Tauc (Plenum, New York, 1974), p. 101.

[4] P. W. Anderson, Phys. Rev. 109, 1492 (1958).

[5] J. C. Phillips, Comments Solid State Phys. 4, 9 (1971).

[6] J. A. Van Vechten, Solid State Commun. 11, 7 (1972).

[7] D. Emin, Phys. Rev. Lett. 28, 604 (1972).

[8] P. W. Anderson, Nature (Lond.) 235, 163 (1972).

[9] P. W. Anderson, Phys. Rev. Lett. 34, 953 (1975).

[10] W. Paul, G. A. N. Connell, and R. J. Temkin, Adv. Phys. 22, 529 (1973).

[11] T. M. Donovan, E. J. Ashley, and W. E. Spicer, Phys. Lett. A 32, 85 (1970); R. F. Willis, L. D. Laude, and B. Fitton, Phys. Rev. Lett. 29, 220 (1972).

[12] A. J. Lewis, G. A. N. Connell, W. Paul, J. R. Pawlik, and R. J. Temkin, in *Proceedings of the International Conference on Tetrahedrally Bonded Amorphous Semiconductors*, edited by M. H. Brodsky, S. Kirkpatrick, and D. Weaire (American Institute of Physics, New York, 1974), p. 27.

[13] S. C. Moss and J. F. Graczyk, Phys. Rev. Lett. 23, 1167 (1969), and Ref. 3, p. 658.

[14] A. J. Lewis (unpublished).

[15] T_s is the platform temperature when rf sputtering is not in progress.

[16] R. J. Temkin, W. Paul, and G. A. N. Connell, Adv. Phys. 22, 581 (1973).

[17] P. M. Grant and W. Paul, J. Appl. Phys. 37, 3110 (1966). The program used in the present study was devised by A. J. Lewis.

[18] G. A. N. Connell, R. J. Temkin, and W. Paul, Adv. Phys. 22, 643 (1973).

[19] G. A. N. Connell and A. J. Lewis, Phys. Status Solidi B 60, 291 (1973).

[20] L. S. Singer, J. Appl. Phys. 30, 1463 (1959).

[21] W. Kaiser and P. H. Keck, J. Appl. Phys. 28, 882 (1957).

[22] W. Kaiser, P. H. Keck, and C. F. Lange, Phys. Rev. 101, 1264 (1956).

[23] I. W. Levin, J. Chem. Phys. 42, 1244 (1965).

[24] M. L. Delwaulle and F. Francois, C. R. Acad. Sci. B 230, 743 (1950).

[25] L. P. Lindeman and M. K. Wilson, Electrochim. Acta 9, 47 (1957).

[26] J. Tauc, A. Abraham, R. Zallen, and M. Slade, J. Non-Cryst. Solids 4, 279 (1970).

[27] R. C. Chittick, J. Non-Cryst. Solids 3, 255 (1970).

[28] E. Burstein, S. Iwasa, and Y. Sawada, Rend. Sc. Int. Fis. "Enrico Fermi" 34, 421 (1966).

[29] T. M. Donovan, W. E. Spicer, J. M. Bennett, and E. J. Ashley, Phys. Rev. B 2, 397 (1970).

[30] T. M. Donovan in Ref. 12, p. 1, see also accompanying discussion of G. A. N. Connell and A. J. Lewis.

[31] J. M. Ziman, J. Phys. C 1, 1532 (1968).

[32] G. E. Becker and G. W. Gobeli, J. Chem. Phys. 38,

2942 (1963).

[33] N. J. Shevchik (unpublished).

[34] G. A. Somorjai, Catal. Rev. 7, 87 (1972).

[35] H. Ibach and J. E. Rowe, Surf. Sci. 43, 481 (1974).

[36] *Handbook of Chemistry and Physics*, 54th *Ed.* (Chemical Rubber Publishing Company, Cleveland, 1973), p. F200.

[37] M. L. Theye (unpublished).

[38] M. H. Brodsky, D. M. Kaplan, and J. F. Ziegler, in *Proceedings of the Eleventh International Conference on Physics of Semiconductors* (PWN-Polish Scientific Publishers, Warsaw, 1972), p. 529.

[39] D. I. Jones, W. E. Spear, and P. G. Le Comber (unpublished).

[40] J. A. Appelbaum and D. R. Hamann, Phys. Rev. Lett. 31, 106 (1973); *ibid.* 32, 225 (1974).

[41] N. F. Mott, E. A. Davis, and R. A. Street (unpublished).

[42] This possibility was suggested to us by D. M. Kaplan.

[43] M. A. Paesler, S. C. Agarwal, S. J. Hudgens, and H. Fritzsche, in Ref. 12, p. 37.

[44] J. R. Pawlik, G. A. N. Connell, and A. J. Lewis (unpublished).

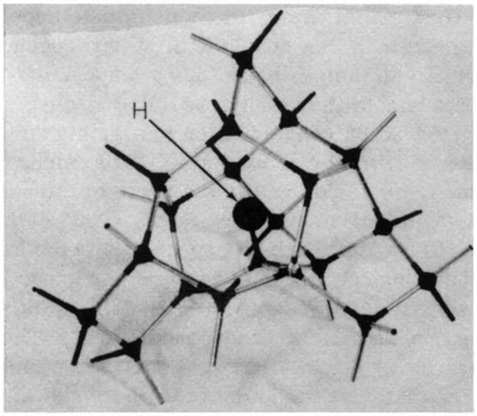

FIG. 7. Example of the network near a bulk-incorporated hydrogen atom.